Journal of Combinatorial Mathematics
and Combinatorial Computing
www.combinatorialpress.com/jcmcc

Combinatorial Press

Oscillation cessation due to removal of Na^+ current restored by external noise stimulation

Xiaoqin Si[1], Dawei Chen[1,]✉

[1] *City University of Hefei, Hefei, Anhui, 238076, China*

ABSTRACT

In this study, a complete two-dimensional anatomical model of the rabbit heart was constructed by Zhang et al. The positive effects of external noise stimulation on cardiac pacemaking and conduction have been studied using computer simulations. Our results show that: 1) the slower pacemaking rate or even oscillation cessation, which is induced by the removal of i_{Na} from the sinoatrial node or a decrease in the active sinoatrial node cell population, can be recovered by adding external noise. 2) Compared to the effect of i_{Na} removal alone, the combined effect of i_{Na} and cell death had a greater impact on slowing down the pacemaking rate. These phenomena indicate that external stimuli play an important role in controlling the initiation and conduction of sinoatrial node pacemaker activity, and that the aging heart may experience obstruction of sinus node conduction and even sudden cardiac death due to decreased cell membrane i_{Na} or partial myocardial cell death. Our results provide insights into the intrinsic mechanisms underlying electroshock healing in some heart diseases.

Keywords: Oscillation cessation, Cardiac recovery, External noise stimulation, Cell death

1. Introduction

Noise in electronic circuits refers to the random signals generated in electronic equipment. These random signals can interfere with normal electronic signal transmission and processing, reducing the performance and reliability of the equipment. In circuit design and application, it is crucial to understand and deal with the problem of noise in circuits [1-4]. In electronic circuits, noise is any voltage or current that is not associated with the desired signal. Noise can be categorized into several different types, such as thermal noise, subrhenian noise and gap noise. The most common of these is thermal noise. Noise interferes with the transmission and processing of normal electronic signals, leading to degradation of signal quality and affecting the performance of electronic systems [5-8].

An oscillator circuit is a circuit capable of generating periodic electrical signals, which has a wide range of applications in electronics. The basic components of an oscillator circuit include an amplifier,

✉ Corresponding author.
E-mail address: sxq0796@163.com (D. Chen).
Received 20 February 2024; Revised 25 April 2024; Accepted 20 November 2024; Published Online 16 April 2025.
DOI: 10.61091/jcmcc127b-475

a feedback circuit and a frequency selection network [9-11]. When the amplifier amplifies the signal in the circuit, the feedback circuit returns part of the signal back to the amplifier, thus forming a closed loop. The frequency selection network is used to select the oscillation frequency of the circuit. In an oscillator circuit, the frequency selection network plays a crucial role [12-15]. It selects the oscillation frequency of the circuit and ensures that the circuit oscillates stably at that frequency. Frequency selective networks are usually composed of capacitors and inductors, which form a resonant loop to select the frequency of oscillation of the circuit. Oscillator circuits are widely used in radio communications, computers, audio equipment and other fields [16-19].

In this study, to evaluate the functional roles of external noise stimulus on the initiation and conduction of pacemaker activity, a series of simulations were performed under i_{Na} removal from SA node conditions, decrease in active SA node cell population, or a combination of both.

Our results showed that abnormal fluctuations in heart rate can be recovered by external noise stimuli and can help the SA node drive the atrial muscle, indicating that external fluctuations play an important role in controlling the initiation and conduction of pacemaker activity. Furthermore, we found that the combined effect of i_{Na} removed and cell death slowed down the pacemaking rate. In addition, we discuss the relationship between i_{Na} and aging.

2. Model development

The pacing activity and conductivity of the heart depend not only on the characteristics of SA node cells and the spatial structure of myocardial cell tissue, but are also closely related to the connection with surrounding myocardial cells and the regulatory role of the nervous system. This study adopted the complete two-dimensional experimental anatomical model of rabbit SA node atrial muscle cells proposed.

Based on the electrophysiological characteristics of cells and experimental data, the dynamic equation of the action potential of each myocardial cell can be expressed as:

$$\frac{dV}{dt} = -\frac{1}{C_m}(i_{Na} + i_{K,ACh} + i_{\text{tot}}) \tag{1}$$

where V is the membrane potential of the cell (in mV), t is the time, C_m is the membrane capacitance of the cell (in μF), i_{Na} is the current of TTX-sensitive Na+, $i_{K,ACh}$ is the current of the acetylcholine-activated potassium channel, and i_{tot} is the total membrane ionic channel current except for i_{Na} and $i_{K,ACh}$ in a cell. The meanings and values of each physical quantity and parameter in the equation are detailed in literature.

The current $i_{K,ACh}$ contains conductivity $g_{K,ACh}$ is closely related to acetylcholine, which satisfies the following equation:

$$i_{K,ACh} = g_{K,ACh}\left(\frac{[K]_e}{10+[K]_e}\right)\times\left(\frac{V_m - E_K}{1+\exp[(V_m - E_K - 140)F/2.5RT]}\right) \tag{2}$$

$$g_{K,ACh} = g_{K,ACh\ \max}\, jk \frac{[ACh]^{n_{K,ACh}}}{K_{0.5,K,ACh}^{n_{K,ACh}} + [ACh]^{n_{K,ACh}}} \tag{3}$$

where $g_{K,ACh}$ is the conductivity (μs), $[K]_e$ is the extracellular potassium ion concentration (in mM), and $[ACh]$ is the acetylcholine concentration (M).

The equation for i_{Na} is as follows:

$$i_{Na} = k \cdot g_{Na} m^3 h \times [Na]_0^+ \frac{VF^2 e^{(V - E_{Na}F/RT)-1}}{e^{VF/RT-1}} \tag{4}$$

where g_{Na} is the conductivity of the sodium ion channel, and k is the gene mutation parameter. As K

changes, it indicates that the sodium ion flow entering the myocardial cells is disrupted, leading to irregular heartbeats and irregular heart rates, which can lead to two common arrhythmic diseases: Brugada syndrome and Q-T interval prolongation syndrome. The former is due to insufficient sodium ions entering the myocardial cells (k<1), whereas the latter is due to excessive sodium ions entering (k>1).

In this model, the effects of slowing down the pacemaking rate or even cessation can be mimicked by removing i_{Na} (k<1) from the SA node, cell death, or the combined action of the two. This model was also modified to show the depressive effect of ACh, a neurotransmitter released by the parasympathetic nervous system, on pacemaking.

A two-dimensional coupled system is constructed by selecting cells that satisfy Equation (1) as the basic unit, as follows:

$$C_m^x(i,j)\frac{dV^x(i,j)}{dt} = -[i_{tot}^x(i,j) + D \times \nabla^2 V^x(i,j)] \tag{5}$$

$$g_{Na}^x(i,j) = \frac{[65 - C_m^x(i,x)]g_{Na,c} + [C_m^x(i,j) - 20]g_{Na,p}}{45} \tag{6}$$

The grid points (i, j) represent the spatial position of each cell, the superscript "x" represents the sinoatrial node or atrial cell, and D represents the gap junction conductance between atrial muscle cells or SA node cells. The second term on the right side of Equation (4) represents the diffusion coupling term between the cells, where each cell is coupled to the four nearest cells.

In this study, a two-dimensional network model of 375×45 was used by coupling cells; such as the sinoatrial node, atrium, and connective tissue. The zero-flux boundary conditions are used to numerically solve equations (4) and (5) by using the five point difference method, with a time step of 0.05ms and a spatial step of 0.04 mm selected.

3. Results and Discussion

3.1. The effect of sodium ion channel current changes on SA node pacing activity

The sodium current i_{Na} in SA node cells is an important parameter for controlling the cardiac rhythm; when i_{Na} decreases, the membrane voltage oscillation of SA node cells weakens or even stops. Simulations have shown that blocking the SA node i_{Na} results in an increase in pacemaking CL (the time interval between two successive pacemaking action potentials) (equivalent to a decrease in pacemaking rate) and SA node-atrium conduction time (SACT). Reduction of i_{Na} can also produce the SA node-atrium conduction block, in which action potentials originating from the SA node fail to conduct into the atrium or terminate the SA node pacemaker activity.

The simulation results reproduce this conclusion, when the sodium conductivity g_{Na} decreases to 90%, 80% and 70% of the original value (k=0.9, 0.8, 0.7), the cycle of action potential (CL) are 370ms, 374ms and 376ms, respectively, an increase of 6ms, 10ms and 12ms compared to the normal g_{Na} vibration period of 364ms, it indicates that the pacing activity of the SA node weakens with a decrease in g_{Na}. When g_{Na} decreased to 60% of its original value (k=0.6), a dead beat occurred in the SA node pacing activity.

When the sodium conductivity g_{Na} increased to 120%, 140%, and 160% of the original value (k=1.2, 1.4, 1.6), the CL values were 354ms, 342ms, and 330ms respectively, a decreases of 10ms, 22ms and 34ms compared to the normal g_{Na} vibration period of 364ms.

The simulation results further indicate that k<1 causes bradycardia or sinus arrest of the SA node pacing activity, whereas K>1 accelerates the pacing activity of the SA node, resulting in sinus tachycardia and atrial fibrillation symptoms.

3.2. The restoration effect of external noise

The pacing activity of SA node cells is regulated by the concentration of ACh secreted by the nervous system, which is influenced by the noise in the external environment of the system. ACh plays a crucial role in the nervous system, by transmitting signals between neurons and by controlling the excitation and inhibition of cells. Therefore, the expression for ACh concentration under the influence of external noise can be described by the following equation:

$$[ACh] = [ACh]_0 \times [1 + \xi(t)] \tag{7}$$

where $[ACh]_0$ can be set as a constant value, 1.0×10^{-7} *M*, and $\xi(t)$ is color noise. Changes in the impact of color noise on the human vagus nerve can be used to obtain the impact of noise on the heart rate, and its differential equation can be expressed as follows:

$$\frac{d\xi(t)}{dt} = [\rho\Gamma(t) - \xi(t)] / \tau \tag{8}$$

Where ρ is the intensity of the colored noise and τ is the correlation time. $\Gamma(t)$ is a Gaussian white noise that satisfies $\langle \Gamma(t)\Gamma(t') \rangle = \sigma^2 \delta(t - t')$ and $\langle \Gamma(t) = 0 \rangle$. Gaussian white noise was randomly generated through a digital simulation using a digital generator.

Cardiac arrest is often the direct cause of sudden cardiac death and is mainly caused by arrhythmias. However, prolonged abnormal pacing activity in the SA node can lead to the clinical symptoms of sudden cardiac death. Immediate cardiac resuscitation and early defibrillation after cardiac arrest are key to preventing death. Therefore, to restore the heart to a normal state, we simulated the disturbance of external environmental color noise to eliminate the dead vibration phenomenon.

We know that the sodium conductivity was adjusted to 60% g_{Na} of normal (k=0.6), the SA node system only vibrated for 2.4s before exhibiting a dead vibration (Figure 1. A). To allow the heart cells to vibrate again and return to a sustained oscillatory state, in the simulation, we introduce colored noise, as shown in equation (6-7) and adjust its noise intensity and correlation time to an appropriate value.

As shown in Figure 1. B, after SA cell oscillation death, the transient colored noise stimulus at the 3rd second position was introduced, and the colored noise stimulus with a length of 3 s. From Figure 1. B, it can be seen that the stimulation of color noise of this intensity did not immediately restore the oscillation of the sinoatrial node, but rather started oscillation after a 3-second interval of action time. Figure 2. A shows the corresponding CL-t graph, and the CL after restoring pacing to noise stimulation is consistent with the normal pacing cycle.

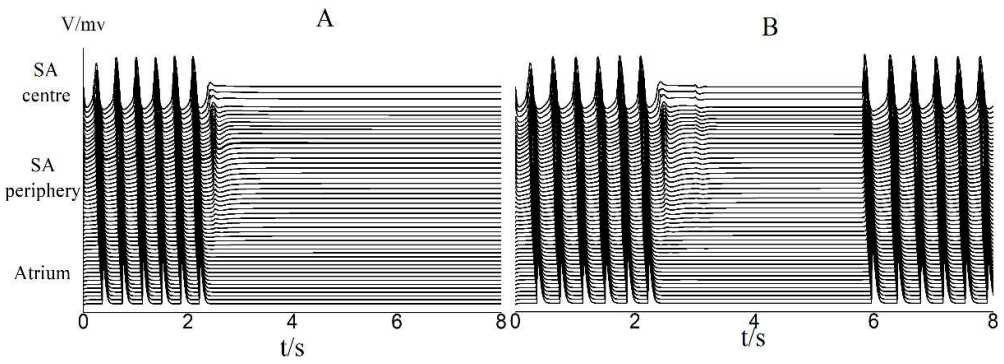

Fig. 1. A. Action potentials recorded from cells with removal of i_{Na} by 60% (k=0.6); Figure 1. B. After the SA cells oscillation death, the colored noise stimulus by the length of 3 seconds is introduced, the noise intensity $\rho = 500$, correlation time $\tau = 3000$.

Further research has found that the stimulus recovery effect of colored noise is related to its correlation time. When the correlation time was 0, color noise stimulation of any noise intensity immediately restored the normal oscillation of the sinoatrial node, without the need for a brief transition time. However, during the stimulation period, the CL value was slightly higher than the normal vibration value, and after the stimulation period, it reached a normal value. As is shown Figure 3. A, Color noise stimulation was introduced at the 3rd second, and external stimulation was stopped at the 6th second. The sinoatrial node begins to oscillate at the 3rd second position, but within 3-6s CL=472ms, the cycle increases and pacing activity slows down. After the 6th second, the normal value returned to 364ms (Figure 2. B).

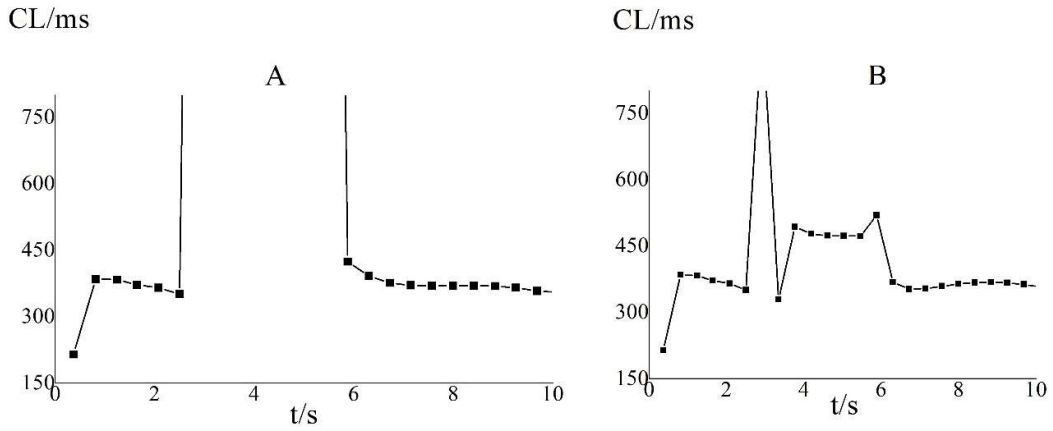

Fig. 2. CL-t plots for different noise effects. A: $\rho = 500$, $\tau = 3000$; B: $\rho = 50$, $\tau = 0$

Compared to the given weak noise intensity, a longer correlation time actually suppresses this restoration effect under the same correlation time; the weaker the noise intensity, the more significant is the inhibitory effect, as shown in Figure 3. B and Figure 3. C. Only when the noise intensity is sufficiently strong and unaffected by the correlation time can the sinus node cells be activated and return to a sustained oscillatory state.

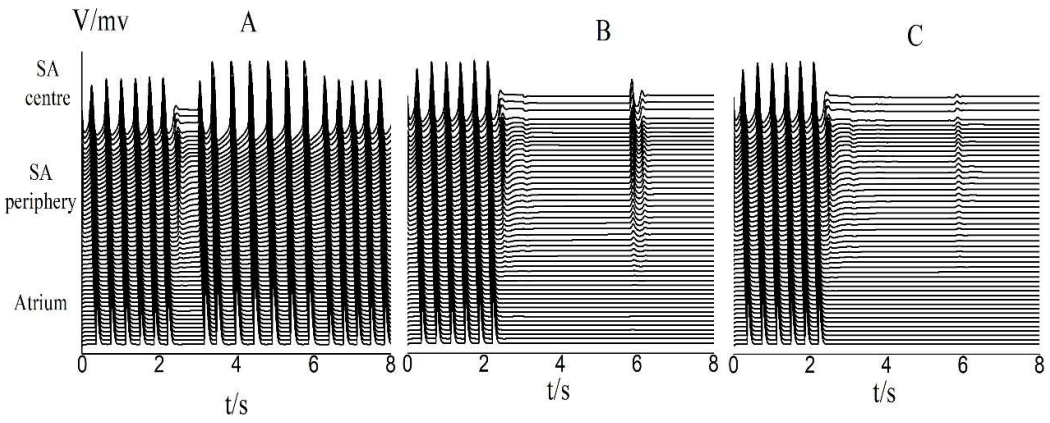

Fig. 3. Oscillation plots of colored noise stimuli with different noise intensities and correlation times. A: $\rho = 50$, $\tau = 0$; B: $\rho = 0.1$, $\tau = 1600$, C: $\rho = 0.02$, $\tau = 1600$

Select the area with weak noise intensity $\rho \le 0.2$ and correlation time $\tau \le 5000$ for a graph of the oscillation region is shown in Figure 4. where I represents an area where vibration cannot start at all, II represents a very brief recovery of vibration, and III represents the complete recovery of the sustained oscillation. From the scientific research in the figure, it can be seen that color noise stimulation with low noise intensity and a large correlation time cannot restore the normal oscillation of the sinoatrial node. A slightly higher level of noise intensity and an appropriate correlation time for noise stimulation can completely restore oscillation.

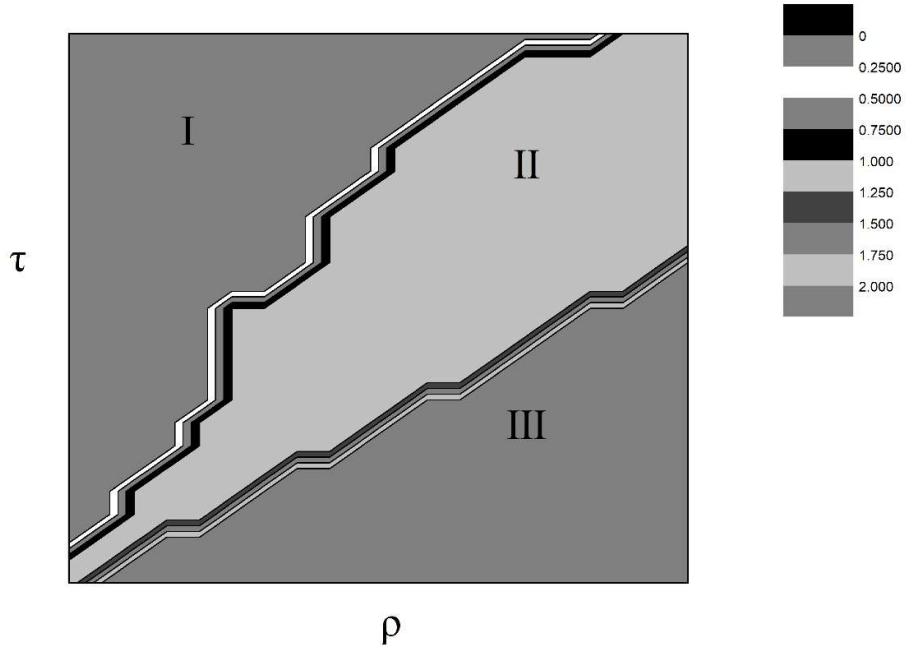

Fig. 4. Oscillation region plots of weak noise intensity and correlation time

The simulation shows that abnormal situations with k<1 can be restored using the colored noise in equation (6-7), but this colored noise with K>1 cannot restore it to its normal state and requires other noises to restore it.

3.3. The effect of the proportion and distribution of dead cells in myocardial cells

A complete two-dimensional network model consisting of 375×45 rabbit sinus nodes and surrounding atrial muscle cells coupled with cells, such as the sinus node, atrium, and connective tissue, is shown in Figure 5 (color). This is a complex system with smaller central cells than peripheral cells and poor tissue connectivity. To study the effect of cell death on cardiac pacing activity, it was first assumed that dead cells were randomly distributed throughout the entire cardiac slice, and the above two-dimensional coupled model was used for the simulation.

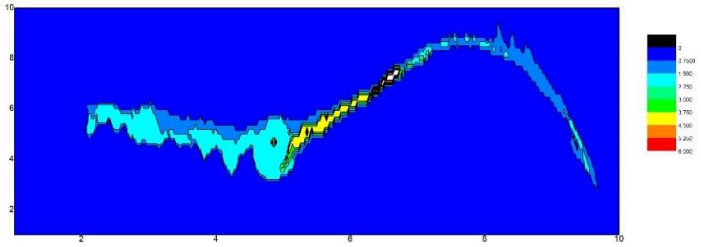

Fig. 5. Two-dimensional network model of a complete rabbit sinus node.

Key cell types: 0, empty 1, connective tissue, 2 atria, 3 SAN periphery, 4 SAN center, 5 blood vessels, 6 block zone

The simulation shows that a decrease in the number of active SA node cells slows down the pacing rate, which is mainly manifested by an increase in the cycle of action potential (CL). The more dead the cells, the greater the CL, which means that the pacing rate of the heart slows down with an increase in the number of active cell deaths. As shown in Figure 6. A, the proportion of dead cells reached 10% (the number of dead cells was 375 × 45 × 10%), with CL=374ms, which was 10ms more than the cell cycle without death CL=364ms. When the number of active cells decreased to 15%, the sinoatrial node lost pacing activity and could not drive the atrial muscle (Figure 6. B), which is similar to the 16% cell death rate reported in elderly patients in clinical practice.

This article also discusses the combined effect of cell death in the SA node and decrease in i_{Na} caused by g_{Na} reduction during SA node pacing. The results show that the combined effect of the two has a greater impact on slowing down the cardiac pacemaking rate and producing impairment of impulse initiation and conduction that leads to SA node-atrium conduction exit block. As shown in Figure 6. C, when 10% of the cells died and sodium conductivity was reduced to a normal 60% (k=0.6) combined effect, the SA node quickly lost pacing activity and could not conduct conduction in time or drive the atrial muscle normally.

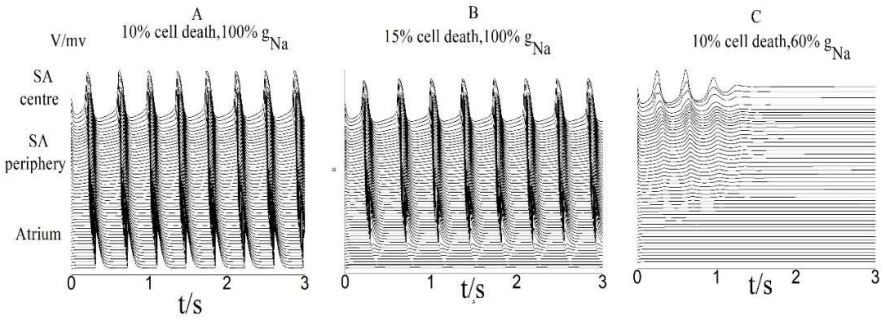

Fig. 6. Schematic diagram of the sinus node pacing signal transduction in the sinoatrial node with different cell death ratios and g_{Na}

Ion flow through the myocardial cell membrane affects the electrical activity of the heart and plays

a crucial role in the cardiac characteristics and function. Changes in the ion flow can cause abnormal conduction of cardiac excitement, leading to arrhythmias. Under normal conditions, i_{Na} participates in the rapid 0-phase depolarization of the action potential. therefore, the pacing activity of SA node cells follows a normal rhythm, and the time series diagram of their i_{Na} is shown in Figure 7. A. If external factors affect the rapid repolarization current of myocardial cells, the inward sodium ion current density decreases, and the depolarization rate slows down. For example, increasing the proportion of dead cells can lead to changes in the i_{Na} and irregular oscillation sequences of i_{Na} (Figure 7. B), and inhibition of pacing activity (Figure 7 C).

It can be said that the decrease in i_{Na} activity in the main channel current may lead to the dead vibration behavior of SA node cells, which means that the pacing and conduction of SA node cells are usually inhibited by the decrease in i_{Na}.

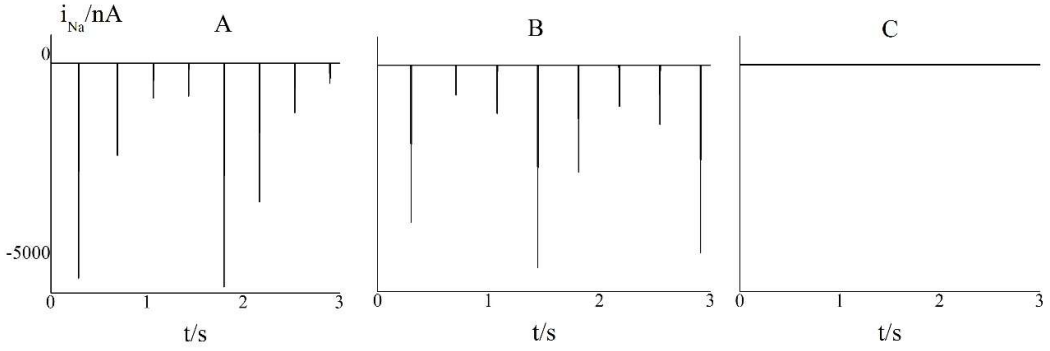

Fig. 7. Time series diagram of i_{Na} recordings from an SA node cell under different conditions. A: No cell death; B: 10% cell death; C: 15% cell death.

4. Conclusions and Discussion

In this study, we used a 2D anatomical model of the intact SA node and atrium to evaluate the functional roles of external noise simulation in driving the SA node. We found that, on the one hand, for an i_{Na} that was removed from the SA node, the color noise resulted in the heart cells initiating and conducting from the time. In contrast, the proportion and distribution of dead myocardial cells slowed the pacing rate. We also found that both dead cells and i_{Na} that removed from the SA node had a remarkable influence on this transition behavior.

The simulation results showed that the disturbance effect of environmental noise is introduced into SA node cells by utilizing the regulatory effect of neurotransmitters secreted by the nervous system. Appropriate environmental noise disturbances allow the SA node to experience dead oscillations and resume oscillations. The restoration effect of noise is only closely related to its intensity and correlation time, and is not directly related to the starting point of the action time.

In conclusion, external noise played an important role in the initiation and conduction of pacemakers. Therefore, our simulation results indicate the possible influence of external noise on the pacemaking of the SA nodes. We hope that our findings will be useful in understanding the properties of SA nodes and the mechanisms of information processing in real human organisms.

Ethical Compliance

All procedures performed in this study involving human participants were in accordance with the ethical standards of the institutional and/or national research committee and with the 1964 Helsinki Declaration and its later amendments or comparable ethical standards.

Data Access Statement

Research data supporting this publication are available from the NN repository at www.NNN.org/download/.

Conflict of Interest Declaration

The authors declare that they have no affiliations with or involvement in any organization or entity with any financial interest in the subject matter or materials discussed in this manuscript.

Funding

This study was supported by the General Project for Outstanding Youth Talent Support Program in Universities of Anhui Province of China (gxyq2022186); the University Youth Teacher Training Action Project of Anhui Province of China (YQZD2024065); the Key Project of University Natural Science Research of Anhui Province of China (2023AH053238); and the major Foundation of University Natural Science Research of Anhui Province of China (KJ2019ZD64).

Reference

[1] Banchuin, R. (2022). Noise analysis of electrical circuits on fractal set. COMPEL-The international journal for computation and mathematics in electrical and electronic engineering, 41(5), 1464-1490.

[2] Urbanek, M., Nachman, B., Pascuzzi, V. R., He, A., Bauer, C. W., & de Jong, W. A. (2021). Mitigating depolarizing noise on quantum computers with noise-estimation circuits. Physical review letters, 127(27), 270502.

[3] Cincio, L., Rudinger, K., Sarovar, M., & Coles, P. J. (2021). Machine learning of noise-resilient quantum circuits. PRX Quantum, 2(1), 010324.

[4] Dalzell, A. M., Hunter-Jones, N., & Brandão, F. G. (2024). Random quantum circuits transform local noise into global white noise. Communications in Mathematical Physics, 405(3), 78.

[5] Fefferman, B., Ghosh, S., Gullans, M., Kuroiwa, K., & Sharma, K. (2024). Effect of nonunital noise on random-circuit sampling. PRX Quantum, 5(3), 030317.

[6] Ren, G., Tang, J., Ma, J., & Xu, Y. (2015). Detection of noise effect on coupled neuronal circuits. Communications in Nonlinear Science and Numerical Simulation, 29(1-3), 170-178.

[7] Ahsan, M., Naqvi, S. A. Z., & Anwer, H. (2022). Quantum circuit engineering for correcting coherent noise. Physical Review A, 105(2), 022428.

[8] Song, Y., & Lee, T. (2017). Electronic noise analyses on organic electronic devices. Journal of Materials Chemistry C, 5(29), 7123-7141.

[9] Marszalek, W., & Sadecki, J. (2018). Complex two-parameter bifurcation diagrams of a simple oscillating circuit. IEEE Transactions on Circuits and Systems II: Express Briefs, 66(4), 687-691.

[10] Takatoh, J., Prevosto, V., Thompson, P. M., Lu, J., Chung, L., Harrahill, A., ... & Wang, F. (2022). The whisking oscillator circuit. Nature, 609(7927), 560-568.

[11] Yoshihara, F., Fuse, T., Ashhab, S., Kakuyanagi, K., Saito, S., & Semba, K. (2017). Superconducting qubit–oscillator circuit beyond the ultrastrong-coupling regime. Nature Physics, 13(1), 44-47.

[12] Elwy, O., Rashad, S. H., Said, L. A., & Radwan, A. G. (2018). Comparison between three approximation methods on oscillator circuits. Microelectronics Journal, 81, 162-178.

[13] Moy, W., Ahmed, I., Chiu, P. W., Moy, J., Sapatnekar, S. S., & Kim, C. H. (2022). A 1,968-node coupled ring oscillator circuit for combinatorial optimization problem solving. Nature Electronics, 5(5), 310-317.

[14] Marszalek, W., Podhaisky, H., & Sadecki, J. (2019). Computing two-parameter bifurcation diagrams for oscillating circuits and systems. IEEE Access, 7, 115829-115835.

[15] Rhea, B. K., Harrison, R. C., Werner, F. T., Perkins, E., & Dean, R. N. (2020). Approximating an exactly solvable chaotic oscillator using a colpitts oscillator circuit. IEEE Transactions on Circuits and Systems II: Express Briefs, 68(3), 1028-1032.

[16] Maheshwari, S., & Verma, R. (2012). Electronically tunable sinusoidal oscillator circuit. Active and Passive Electronic Components, 2012(1), 719376.

[17] Nishio, Y. (Ed.). (2016). Oscillator circuits: frontiers in design, analysis and applications. IET.

[18] Liu, Y., Xia, T., & Li, D. (2021). Hybrid DC circuit breaker based on oscillation circuit. Journal of Power Electronics, 21, 214-223.

[19] Li, H., Li, C., & He, S. (2023). Locally active memristor with variable parameters and its oscillation circuit. International Journal of Bifurcation and Chaos, 33(03), 2350032.